Available online at www.sciencedirect.com
ScienceDirect
Journal of Power Sources 181 (2008) 237–243
JOURNAL OF POWER SOURCES
www.elsevier.com/locate/jpowsour

Embedded flexible micro-sensors in MEA for measuring temperature and humidity in a micro-fuel cell

Chi-Yuan Lee *, Wei-Jung Hsieh, Guan-Wei Wu

Department of Mechanical Engineering, Yuan Ze Fuel Cell Center, Yuan Ze University, 135 FarEast Road, NeiLi, TaoYuan, Taiwan, ROC

Received 30 September 2007; received in revised form 3 January 2008; accepted 4 January 2008
Available online 17 January 2008

Abstract

In this investigation, flexible sensors embedded in a membrane electrode assembly (MEA) are fabricated to measure the temperature and humidity of a micro-fuel cell. Fuel cell performance was determined by the temperature and humidity of the MEA. Restrictions on the sensor volume are such that in previous investigations the temperature and the humidity of the MEA have been measured only at the fuel inlet and outlet. Hence, flexible micro-thin film sensors were fabricated using micro-electro-mechanical systems (MEMS) fabrication technology.

The thin film flexible sensor was 2 μm thick. The temperature and humidity sensors had areas of 180 μm × 180 μm and 180 μm × 220 μm, respectively. A flow channel was integrated in a stainless-steel base (SS-304) with micro-channels that are 300 μm wide and 200 μm deep using wet-etching technology. This study reveals the feasibility of utilizing flexible thin film sensors with micro-fuel cells to measure local temperature and humidity in an MEA. We found that the maximum temperature difference between MEA and the outer surface of a bipolar plate is 5.7 °C. The optimal performance curves of the single cell are obtained at 50 °C, 75%RH and H_2/O_2 gas flow rates of 50 ml min^{-1}. The maximum power density of the fuel cell was 358 mW cm^{-2} and the current density was 796 mA cm^{-2} when the cell voltage was 0.45 V.

Keywords: Embedded flexible micro-sensor; MEMS; MEA

1. Introduction

In recent years, problems associated with energy shortages have become increasingly serious, driving the promotion of green energy. Fuel cells are the most likely technology to replace petrochemical fuel technology and become the main source of energy in the future. However, they still suffer from such problems as low power density, high cost, poor long-term stability and the difficulties of in situ monitoring of the fuel cell's chemical and physical characteristics. Water and heat management are critical determinants of the performance of the fuel cell [1,2]. The temperature and humidity conditions of a membrane electrode assembly (MEA) strongly affects the performance of fuel cells [3]. MEA performs well since its ionic conductivity and gas reaction rate increase with temperature. When the MEA is at low humidity, it cannot be easily traversed by protons. Although water generated at the cathode can wet the MEA, it obstructs the distribution of feed gas when water floods the flow channel, and the performance of the fuel cell worsens significantly as the gas pressure falls.

The volume of traditional temperature and humidity sensors is too large to enable their use in the measurement of temperature and humidity in the MEA of fuel cells. Measurements cannot necessarily be made wherever required. Such sensors measure only the temperature and the humidity outside the fuel cells and yield results with errors that exceed those associated with measurements made in MEA. Several studies have been conducted in this area to monitor the temperature and humidity of fuel cells [4–8]. Some of these works adopted larger commercial sensors [9] to monitor the exterior of fuel cells. Others have used sensors that could be placed at the gas inlet and outlet but not inside the fuel cell. However, they could not measure the temperature or humidity at each local spot inside the fuel cell; they could take only the average value. To date, the simulation of various methods has been studied via computable approaches

* Corresponding author at: Department of Mechanical Engineering, Yuan Ze University, 135 Yuan-Tung Road, Chungli, 320 TaoYuan, Taiwan, ROC. Tel.: +886 3 4638800x2478; fax: +886 3 4558013.
E-mail address: cylee@saturn.yzu.edu.tw (C.-Y. Lee).

0378-7753/$ – see front matter © 2008 Elsevier B.V. All rights reserved.
doi:10.1016/j.jpowsour.2008.01.020

[10–14]. By setting ideal assumption to simple mathematical formulas, simulation can only predict the tendency of temperature and humidity distribution inside the fuel cell. To the best of the authors' knowledge, no research has been performed on the simultaneous monitoring of both temperature and humidity in situ. A traditional thermocouple is typically adopted to measure the temperature of a fuel cell. The sensor has a large volume, so the measurement position cannot be identified precisely, and fuel leaks out during fuel cell assembly. In authors' other research, it was found that the maximum temperature difference between ribs and the outer surface of a bipolar plate was 4.54 °C [15]. This new work reveals the feasibility of utilizing flexible thin film sensors with micro-fuel cells to measure local temperature and humidity in an MEA not ribs.

Due to performance levels and dry or flooding problems in fuel cells, temperature and humidity are important factors. In this investigation, micro-electro-mechanical-systems (MEMS) fabrication technology was utilized to fabricate micro-temperature and humidity sensors on a parylene substrate [16–18] for the purpose of monitoring in situ the temperature and humidity in a fuel cell in MEA. This fabrication technique offers the advantages of (1) mass production, (2) small size, and (3) flexible but precise measurement positions.

2. Methodology

2.1. Theory governing temperature sensors

In this investigation, a resistance temperature detector (RTD) was used as a temperature sensor. The resistance of an RTD increases with the environmental temperature, because a metal conductor has a positive temperature coefficient (PTC). If the temperature variation of RTD is linear, then the relationship between the measured resistance and temperature change is given by

$$R_t = R_i(1 + \alpha_T \, \Delta T) \tag{1}$$

$$\Delta T = t - t_i \tag{2}$$

where R_t and R_i are the resistance of RTD at t (°C) and i (°C); α_T is the positive temperature coefficient of RTD; ΔT is the variation of temperature with the reference temperature; t and t_i are the temperatures of RTD at t (°C) and i (°C). Eq. (1) can be rearranged into

$$\alpha_T = \frac{R_t - R_i}{R_i \, \Delta T} \tag{3}$$

where α_T represents the sensitivity of the temperature sensor ($^\circ C^{-1}$) [19,20].

2.2. Theory governing humidity sensors

Polymeric humidity sensors may be divided into resistive and capacitive sensors according to their constituent polymer. Since temperature affects resistive sensors, capacitive humidity sensors, whose electrode structures are interdigitated, are employed herein. The dielectric constant increases with environmental humidity as the polymer absorbs water. The variation in the capacitance of a humidity sensor is given by

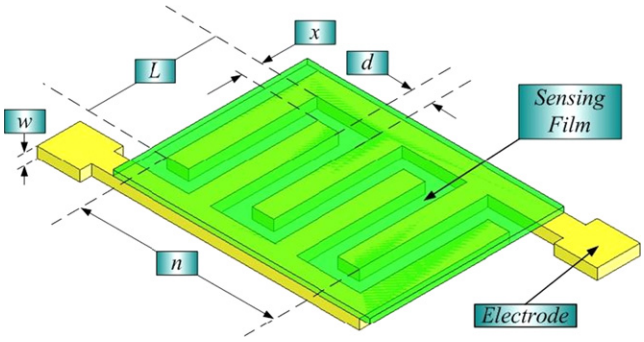

Fig. 1. The structure of micro-humidity sensor.

$$C = n\varepsilon \frac{w(L - x)}{d} \tag{4}$$

where C is the capacitance of the humidity sensor; n is the number of fingers of the interdigitated electrodes; ε is the dielectric constant of the sensing film; w and L are the thickness and the length of the interdigitated electrode, and x and d are the distance between the two electrodes in different directions. Fig. 1 depicts the structure of the capacitive humidity sensor, and the sensitivity of the humidity sensor is given by

$$\alpha_H = \frac{\Delta C}{\Delta \%\mathrm{RH}} \tag{5}$$

where α_H is the sensitivity of the humidity sensor (F/%RH) [19,21].

3. Fabrication

3.1. Schematic of entire system

Figs. 2 and 3schematically depict the entire system and the placement of sensors. We used commercial GDE (E-TEK, LT140EWSI) and Nafion-212 to assemble the MEA. Fig. 4 displays the bipolar plate with the micro-channels. The width

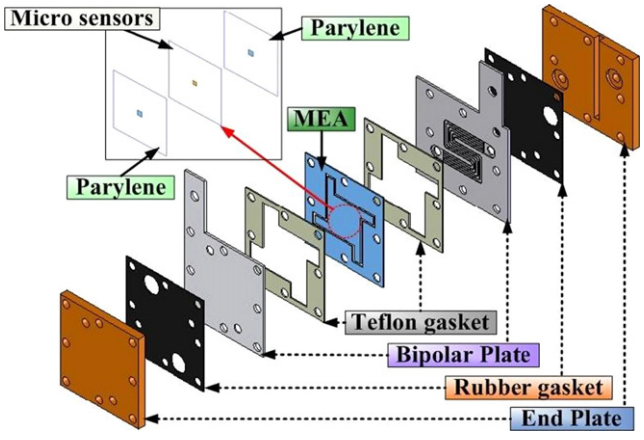

Fig. 2. Schematic of entire system.

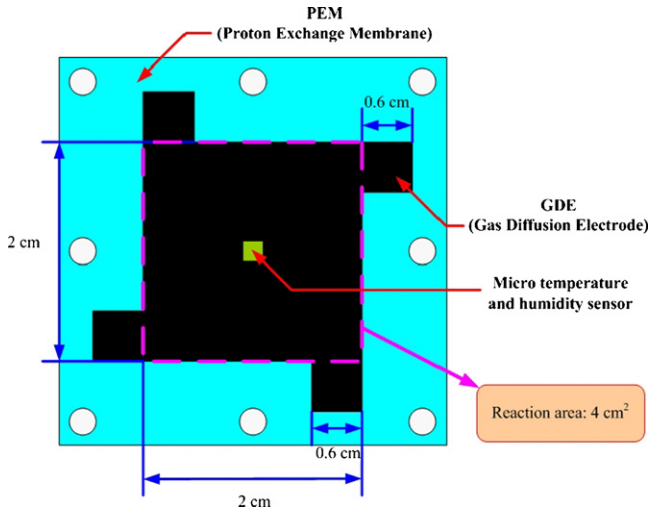

Fig. 3. Placement of sensors.

of each channel is 300 μm, and the depth is 200 μm. To first confirm our initial conception and also considered the total reaction area, we put only one batch of micro-sensors (including one micro-temperature sensor and one micro-humidity sensor) into the center of MEA. When a proton passes through MEA from the anode to the cathode, the chemical reaction increases the temperature of MEA and water is generated at the cathode. The micro-temperature and humidity sensors are placed in MEA to precisely measure the temperature and humidity of MEA at different flow channel positions in situ. The two poly-*para*-xylylene(parylene) thin films are used to protect micro-sensors from the stretching force associated with MEA.

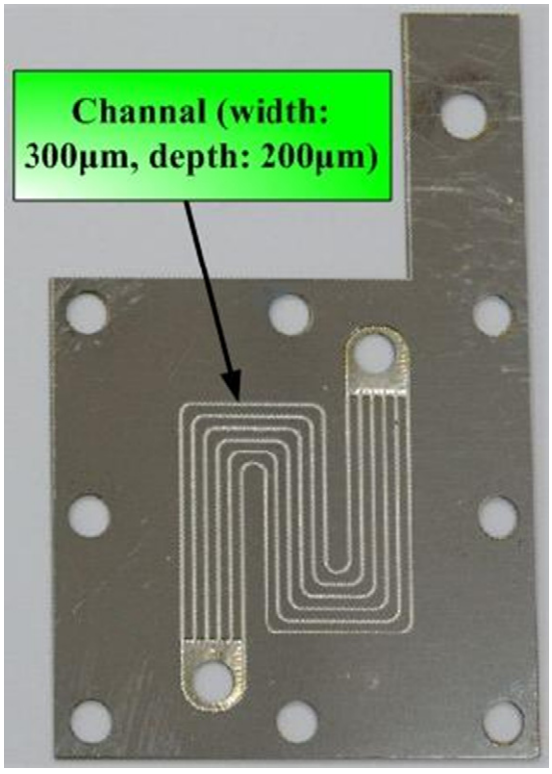

Fig. 4. Bipolar plate with micro-channels.

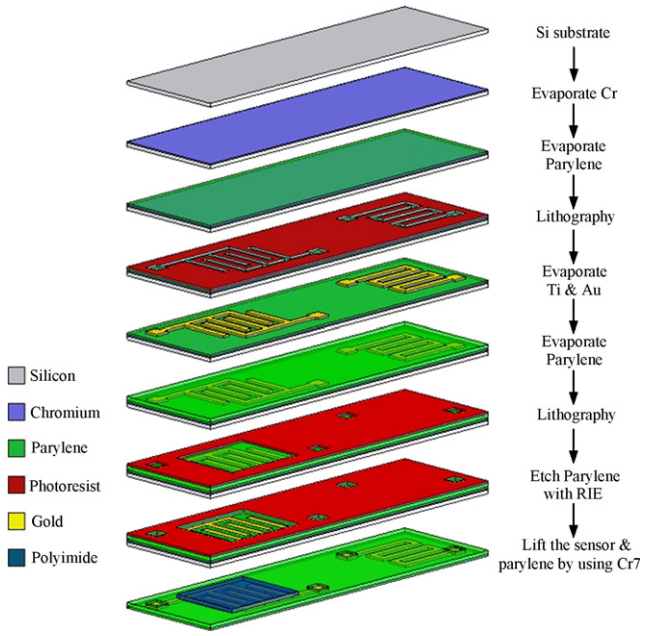

Fig. 5. Fabrication flowchart of parylene-based micro-temperature and humidity sensors.

3.2. Fabrication process of micro-sensors

Fig. 5 shows the fabrication flowchart of parylene-based micro-temperature and humidity sensors. The process begins with the evaporation of a layer of chromium (Cr) on a silicon wafer as a sacrificial layer and the deposition of a 1-μm-thick thin film of polymer parylene as both a protective layer and a substrate. The first lithographic process is applied with the purpose of defining the pattern of the micro-temperature and humidity sensors. Ti (100 Å) and Au (1000 Å) are deposited in that order on parylene substrate using an e-beam evaporator. The structure of the sensors is formed during the lift off process. Then, another parylene layer is evaporated to protect the structure. The second lithographic process is implemented to define the pattern of the contact pads and the sensing region of the film.

Following reactive ion etching (RIE), polyimide is coated on micro-humidity sensor as a sensing film. Finally, the silicon substrate is segmented using a dicing saw and the micro-sensors are peeled by soaking them in chromium etchant.

4. Result and discussion

In this study, the micro-temperature sensor is the gold RTD and the micro-humidity sensor is the capacitive-type sensor with interdigitated electrodes; Figs. 6 and 7 present optical microscopic photographs. The dimensions of the micro-temperature and humidity sensors were 180 μm × 180 μm and 180 μm × 220 μm, respectively. Fig. 8 depicts the final sensor products.

After the sensor had been formed, they were calibrated using a programmable temperature and humidity chamber, which is

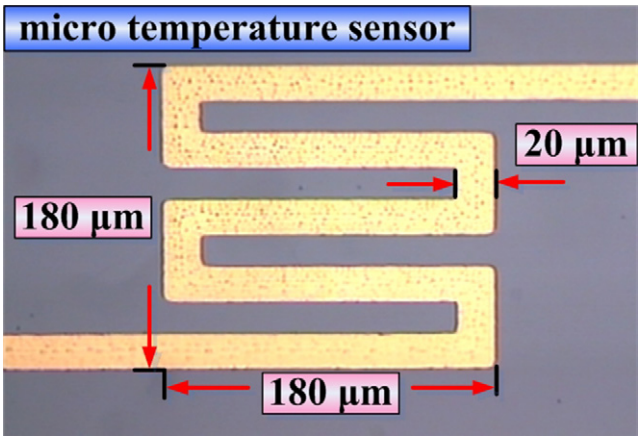

Fig. 6. Optical microscopic photograph of micro-temperature sensor.

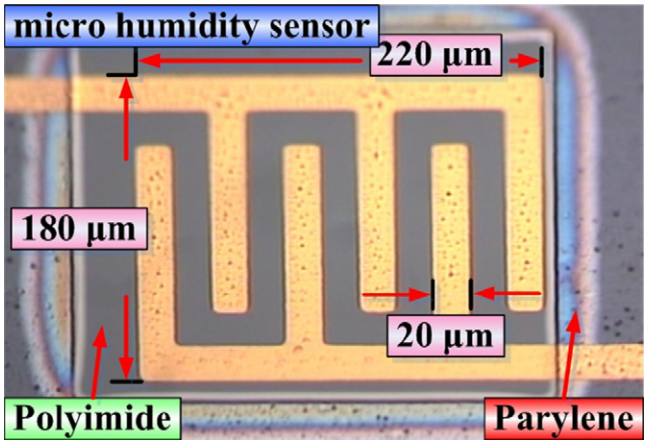

Fig. 7. Optical microscopic photograph of micro-humidity sensor.

shown in Fig. 9. Figs. 10 and 11 plot the calibration curves. The sensitivities of the micro-temperature and the humidity sensor are $4.81 \times 10^{-3}\,^{\circ}C^{-1}$ and 0.03 pF/%RH, respectively.

The micro-temperature and humidity sensors were hot-pressed into MEA. The temperature, humidity and the cell performance were measured using a fuel cell testing system during the operation of the fuel cell, as shown in Fig. 12. Fig. 13 compares the measurements made with the thermocouple and those made with the micro-temperature sensor during the operation of the micro-fuel cell. After 16 min of operations, the temperature measured by the thermocouple was 52.6 °C, and that measured by the micro-temperature sensor was 58.3 °C. We found that the maximum temperature difference between the MEA and the outer surface of bipolar plate is 5.7 °C. Five minutes later, the relative humidity was 94.7%RH, as shown in Fig. 14. We can measure the local temperature and humidity within the MEA but not only takes the average.

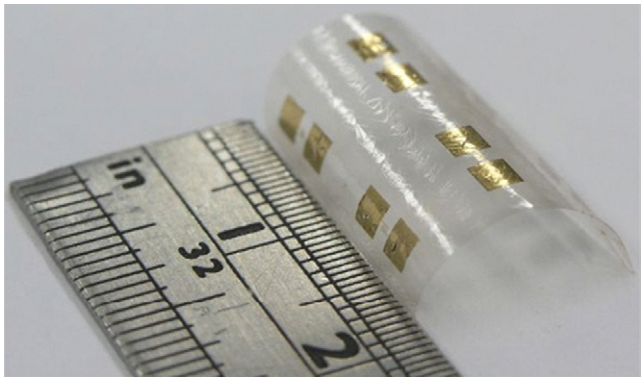

Fig. 8. Final sensor products.

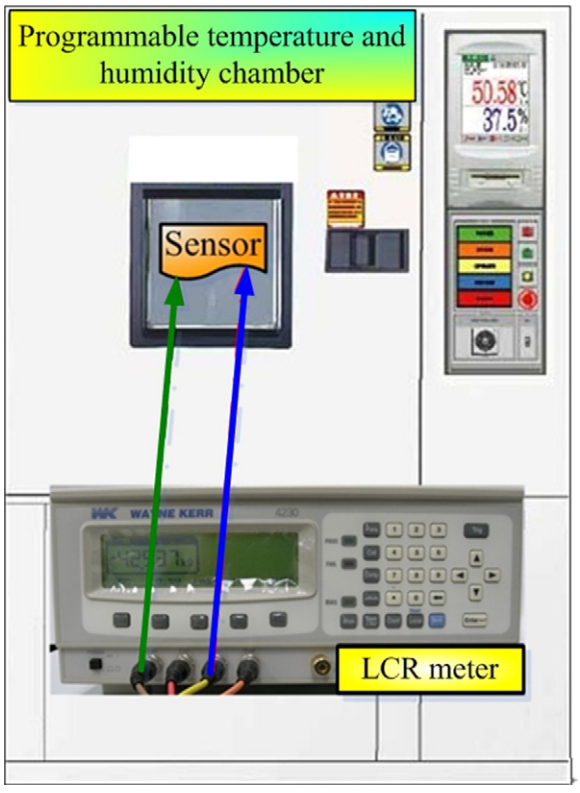

Fig. 9. Programmable temperature and humidity chamber.

Operating conditions seriously influence cell performance. In this investigation, the effects of operating conditions are examined. As indicated in Table 1, three parameters—gas flow rate, humidity, and operating temperatures were studied.

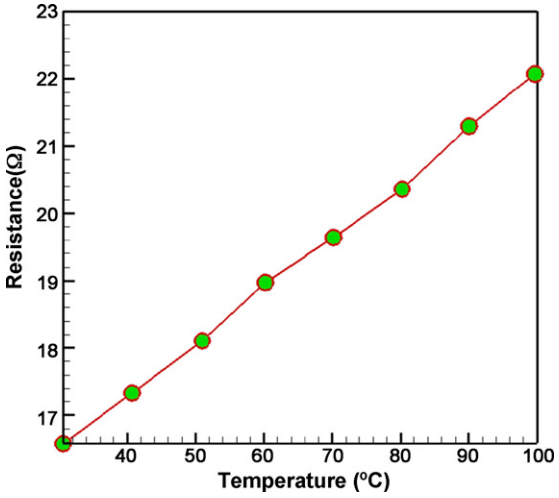

Fig. 10. Calibration curve of micro-temperature sensor.

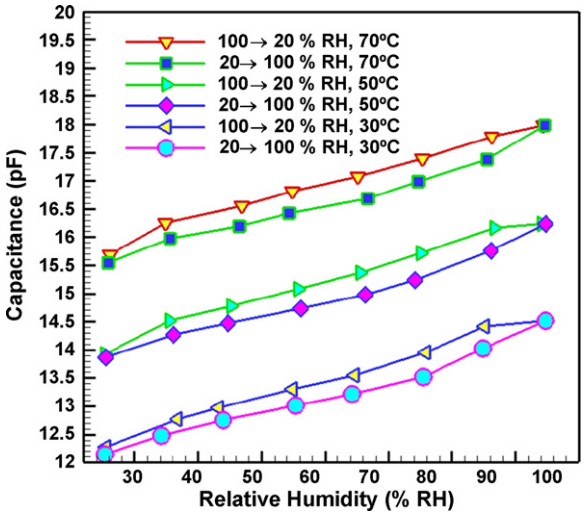

Fig. 11. Calibration curve of micro-humidity sensor.

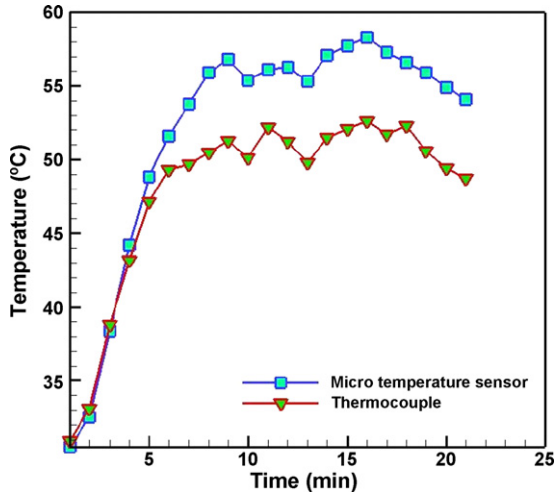

Fig. 13. Comparison of measurements made using thermocouple and micro-temperature sensor during the operation of a micro-fuel cell.

Table 1
Various operating conditions for micro-fuel cell

1. T_{cell} = 50 °C, no humidify Different H_2/O_2 flow rate (ml min^{-1})	30	50	70
2. T_{cell} = 50 °C, H_2/O_2 = 50 ml min^{-1} Different humidify (%RH)	50	75	100
3. No humidify, H_2/O_2 = 50 ml min^{-1} Different operating temperature (°C)	30	50	70

In this work, the performance curves of a single cell were found to be optimal at 50 °C, 75%RH and H_2/O_2 gas flow rates of 50 ml min^{-1}. The maximum power density of the micro-fuel cell was 358 mW cm^{-2} and the current density was 796 mA cm^{-2} at a cell voltage of 0.45 V. Figs. 15–17 plot the data and since flexible sensors were included in the MEA. As displayed in Fig. 18, the insulated parylene film probably reduced the reaction area and also reduced the cells performance.

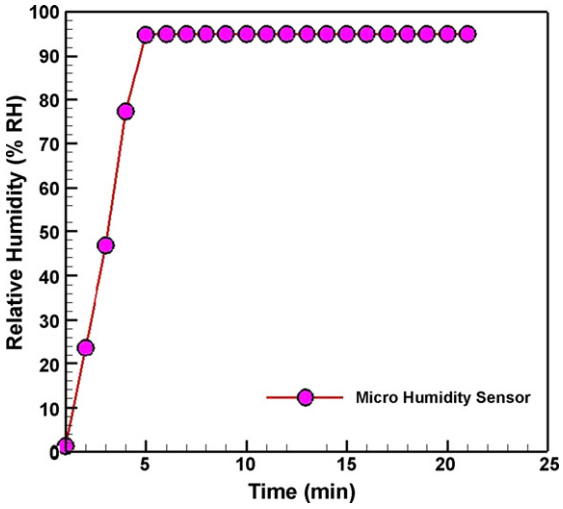

Fig. 14. Humidity measurement using micro-humidity sensor.

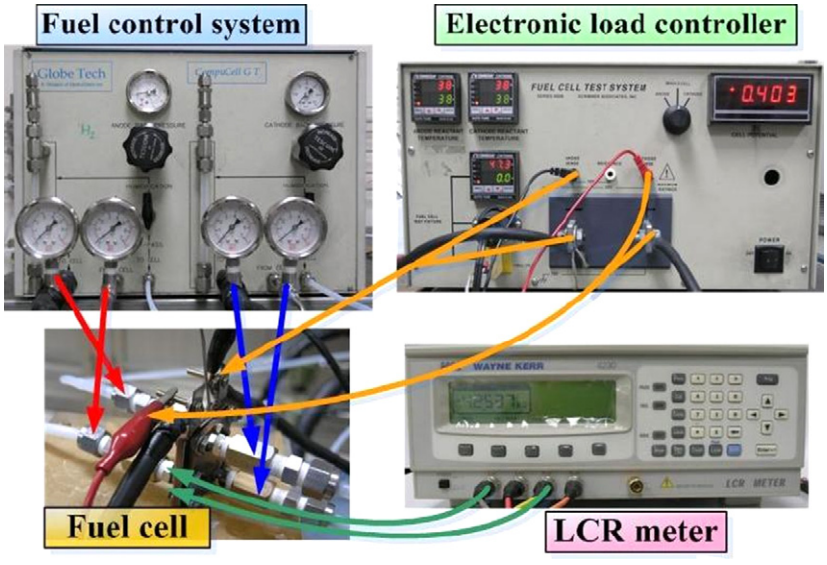

Fig. 12. Fuel cell testing system.

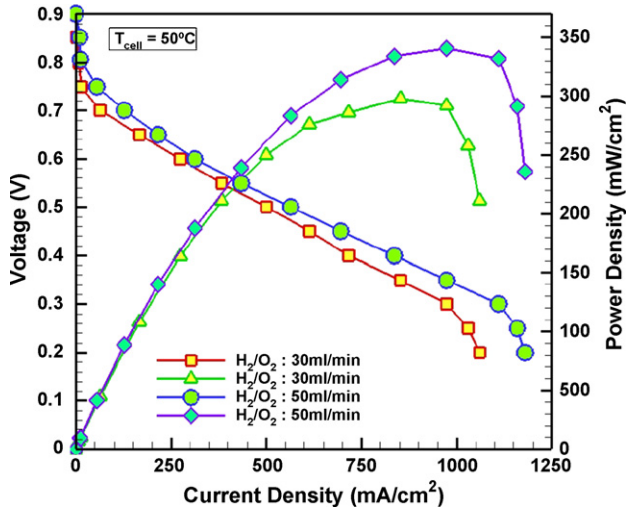

Fig. 15. Variation of cell performance with gas flow rate.

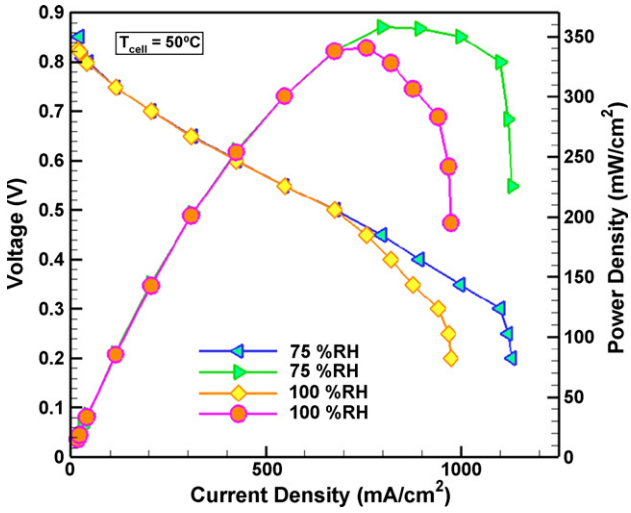

Fig. 16. Variation of cell performance with humidity.

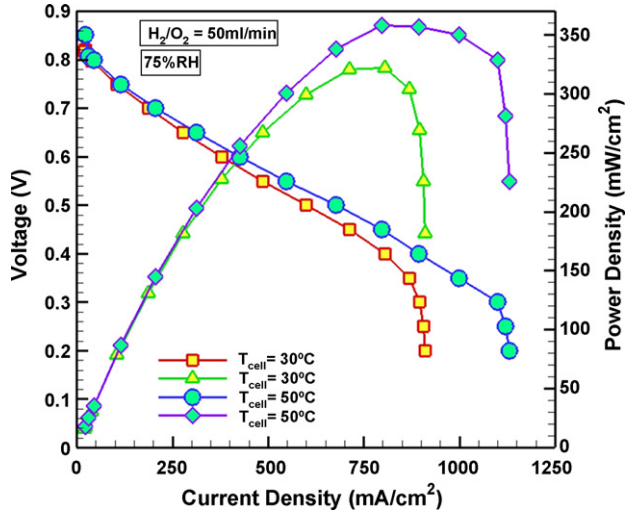

Fig. 17. Variation of cell performance with temperature.

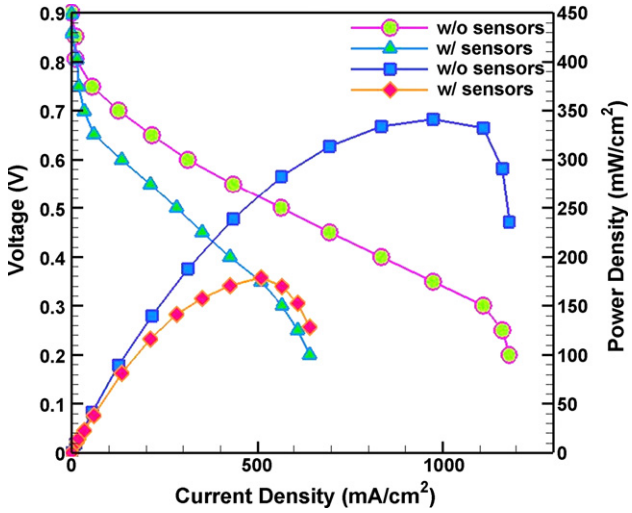

Fig. 18. Comparison of cell performance with and without sensors.

5. Conclusion

In this work, micro-flexible temperature and humidity sensors were successfully fabricated on parylene substrate. Micro-flexible temperature and humidity sensors were employed in situ to monitor the temperature and humidity of a fuel cell within MEA. This technique will provide the optimal operation parameters of fuel cells as references for optimizing maximum cell performance. They will also be used in commercial fuel cells.

Acknowledgements

This work was accomplished with much needed support and the authors would like to thank the financial support of this research from the aim for the top university project of Ministry of Education of R.O.C. and YZU Fuel Cell Center through the Grant No. 0950026846. The authors also like to thank Profs. Lung-Jieh Yang, Shuo-Jen Lee, Shih Hung Chan, Ay Su, Fangbor Weng, Guo Bin Jung for their valuable advice and assistance in experiment. In addition, we would like to thank the TKU MEMS Lab, YZU Fuel Cell Center and NTU NMES Research Center for providing access to their research facilities.

References

[1] J. Larminie, A. Dicks, Fuel Cell Systems Explained, 2nd ed., John Wiley & Sons Ltd., England, 2003.
[2] E.A. Cho, J.J. Ko, H.Y. Ha, S.A. Hong, K.Y. Lee, T.W. Lim, I.H. Oh, J. Electrochem. Soc. 151 (2004) A661.
[3] W. Vielstich, A. Lamm, H.A. Gasteiger, Handbook of Fuel Cells: Fundamentals, Technology, and Applications, Wiley, 2003.
[4] H. Guo, C.F. Ma, M.H. Wang, J. Yu, X. Liu, F. Ye, C.Y. Wang, Proceedings of the First International Conference on Fuel Cell Science Engineering and Technology, Rochester NY, April, 2003.
[5] P.J.S. Vie, S. Kjelstrup, Electrochim. Acta 49 (2004) 1069.
[6] S. He, M.M. Mench, S. Tadigadap, Sens. Actuators A 125 (2006) 170.
[7] M.M. Mench, D.J. Burford, T.W. Davis, Proceedings of IMECE'03 2003 ASME International Mechanical Engineering Congress & Exposition, Washington, DC, November 16–21, 2003.

[8] D.J. Burford, Real-time electrolyte temperature measurement in an operating polymer electrolyte membrane fuel cell, Master Thesis, The Pennsylvania State University, University Park, 2004.
[9] H. Nishikawa, R. Kurihara, S. Sukemori, T. Sugawara, H. Kobayasi, S. Abe, T. Aoki, Y. Ogami, A. Matsunaga, J. Power Sources 155 (2006) 213.
[10] Y. Wang, C.Y. Wang, J. Power Sources 153 (2006) 130.
[11] Y. Wang, C.Y. Wang, J. Power Sources 147 (2005) 148.
[12] Z.X. Liu, Z.Q. Mao, C. Wang, W.L. Zhuge, Y.J. Zhang, J. Power Sources 160 (2006) 1111.
[13] A.A. Shah, G.S. Kim, P.C. Sui, D. Harvey, J. Power Sources 163 (2007) 793.
[14] A. Vorobev, O. Zikanov, T. Shamim, J. Power Sources 166 (2007) 92.
[15] C.Y. Lee, G.W. Wu, C.L. Hsieh, J. Power Sources 172 (2007) 363.
[16] Z. Fan, J.M. Engel, J. Chen, C. Liu, J. Microelectromech. Syst. 13 (2004) 484.
[17] A. Huang, J. Lew, Y. Xu, Y.C. Tai, C.M. Ho, IEEE Sens. J. 4 (2004) 494.
[18] S. Satyanarayana, D.T. McCormick, A. Majumdar, Sens. Actuators B 115 (2006) 494.
[19] J.S. Wilson, Sensor Technology Handbook, Butterworth–Heinemann, 2004.
[20] A.O. Hero, Foundations and Applications of Sensor Management, Springer Verlag, 2007.
[21] C.L. Dai, Sens. Actuators B 122 (2007) 375.